Journal of Crystal Growth 523 (2019) 125159

Contents lists available at ScienceDirect

Journal of Crystal Growth

journal homepage: www.elsevier.com/locate/jcrysgro

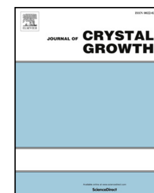

AlGaN multiple quantum wells by PA-MBE for deep UV emission: Effect of growth interruptions

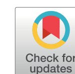

Sayantani Sen[a], Chirantan Singha[a], Anirban Saha[b], Alakananda Das[b], Pushan Guha Roy[b], Pallabi Pramanik[c], A. Bhattacharyya[b,*]

[a] Centre for Research in Nanoscience and Nanotechnology, University of Calcutta, Kolkata 700106, India
[b] Institute of Radio Physics and Electronics, University of Calcutta, Kolkata 700009, India
[c] Department of Electronics and Telecommunication Engineering, Indian Institute of Engineering Science and Technology, Shibpur, Howrah 711103, India

ARTICLE INFO

Communicated by E. Calleja

Keywords:
A1. Interfaces
A1. X-ray diffraction
A3. Migration enhanced epitaxy
A3. Molecular beam epitaxy
B1. Nitrides
B2. Semiconducting III-V materials

ABSTRACT

Growth of AlGaN multiple quantum wells by Plasma Assisted-Molecular Beam Epitaxy has been optimized for use in deep ultraviolet light emitting diodes. A series of samples were grown on c-plane sapphire using an AlN buffer layer, an ~1 µm AlGaN layer, followed by 40-pairs of wells and barriers. The III/V flux ratio was varied from near stoichiometric to excess group III and a plasma exposure step was introduced for some samples after the deposition of wells and barriers. The quality of the well-barrier interface was estimated by the number and intensity of X-Ray Diffraction (XRD) superlattice peaks. Our results indicate that interface abruptness is greatly enhanced by the addition of this process step. While the room temperature photoluminescence (PL) intensity increases significantly upon introduction of the interruption after the barrier layer, this effect is reversed with additional interruption after the well layers. Temperature dependent PL measurements show an anomalous variation with increasing temperature with a maxima around 110°-150°C. This is due to photogeneration of e-h pairs in the underlying AlGaN layer and its subsequent recombination in the quantum wells by diffusion through percolative barrier layers with in-plane potential fluctuations. This is arrested at lowest temperatures causing a reduction in PL intensity. The PL intensity ratio I_{300K}/I_{4K} is highest for samples grown under excess group III, but reduces with the addition of the growth interruption step after the barrier layer. Growth under stoichiometric conditions together with dual growth interruptions was found to be optimal, with improved PL properties while maintaining high interface quality.

1. Introduction

Development of ultraviolet light emitting diodes (UV LEDs) based on high Aluminum content AlGaN alloys has been carried out for a long time, and significant advances have been made [1]. However, the efficiencies are still considerably below those reported for the InGaN alloy based blue LEDs, which has been linked to a number of possible causes [2,3]. Firstly, the lack of lattice-matched substrates that are transparent to the emitted radiation is even more pronounced for these devices, as both GaN templates and SiC substrates are absorbing, leaving sapphire and AlN templates as the only alternatives. While heteroepitaxial growth has been shown to lead to threading dislocations and non-radiative recombination centers associated with them, in InGaN alloys these effects are mitigated by various factors, including spinodal decomposition leading to compositional inhomogeneities [2], or presence of V-defects surrounding the dislocations that generate spontaneously formed potential barriers [3]. Of these, spinodal decomposition is absent in AlGaN alloys due to the similarity of the atomic sizes [4].

This paper focuses on two possible routes to systematic introduction of carrier trapping mechanisms in AlGaN Multiple Quantum Wells (MQWs) designed for the active region of UV emitters in the 235–245 nm wavelength range. The first is the introduction of a controlled amount of compositional inhomogeneity in the AlGaN alloys and the related trapping of carriers at the local potential minima. The second is the creation of "wrinkled" quantum wells, where instead of a smooth surface and interface, a controlled degree of faceting has been deliberately introduced. This second technique will not only cause the formation of quantum wells with variation in thicknesses, but also tilt away from the 0001 direction. This is expected to improve carrier localization as well as the extraction efficiency [5]. Both of these phenomena, compositional inhomogeneity and surface faceting, are

* Corresponding author.
E-mail address: anirban.rpe@caluniv.ac.in (A. Bhattacharyya).

https://doi.org/10.1016/j.jcrysgro.2019.125159
Received 27 March 2019; Received in revised form 4 July 2019; Accepted 18 July 2019
Available online 19 July 2019
0022-0248/ © 2019 Elsevier B.V. All rights reserved.

controlled by the diffusion length of adatoms during deposition, and therefore they are interlinked to a certain degree.

In this work, growth was carried out using Plasma Assisted-Molecular Beam Epitaxy (PA-MBE). This technique has previously produced high internal quantum efficiencies (IQE) in AlGaN/AlN MQWs [6], as well as UV LEDs with reasonable power outputs [7]. The inherent advantage of the MBE technique is the ability to grow materials at significantly lower substrate temperatures, and under very wide range of the group III to group V flux ratios. Furthermore, the interface qualities are significantly better and the Reflection High Energy Electron Diffraction (RHEED) pattern provides a real time monitoring of the same.

A number of alloy phenomena has been reported for AlGaN materials deposited on to sapphire using MBE, including long range atomic ordering, which causes spontaneous superlattice formation along the growth direction [8]. The surface morphology as well as the nanoscale alloy composition is controlled by the diffusion length of the Ga and Al adatoms during growth, and this can be reproducibly controlled by the ratio of their arrival rates to that of active nitrogen. Early work in GaN had established that growth under excess group III leads to smoother surfaces [9], which is true in the broader picture for AlGaN alloys as well. However, excess group III has also been linked to compositional fluctuations in AlGaN alloys, both in the form of spontaneous vertical superlattice structures as well as in-plane fluctuations [8,9]. On the same note, growth under excess group V has been linked to rough and faceted surfaces in GaN [10], and to strong compositional inhomogeneity in AlGaN arising from the limited mobility of the Al adatoms [11]. Furthermore, growth in the excess group V regime is also associated with large dislocation densities [12]. Therefore, in this paper, we have limited our parameter space to only the stoichiometric and excess group III domain.

An additional parameter was investigated during this work. After the deposition of the barrier, or both the well and the barrier, the as-deposited surface was exposed at the growth temperature to active nitrogen plasma in order to modify the surface morphology and hence interface roughness.

2. Experimental details

AlGaN samples were grown in a VEECO Gen 930 MBE system. The Aluminium and Gallium used in this work were of 6N5 and 7N purity respectively. The Nitrogen gas was of 6N5 purity and it was further purified by GATEKEEPER™ filters before being activated by a DC RF plasma source. Growth was carried out on two-inch diameter c-plane sapphire substrates from Monocrystal.

The growth was monitored in-situ using RHEED. Post-growth, the samples were studied by X-ray diffraction (XRD) techniques using a Rigaku SmartLab 9 kW rotating anode XRD system. Optical Transmission measurements were carried out using a Perkin Elmer LAMBDA 1050 spectrophotometer. Temperature dependent photoluminescence (PL) spectroscopy was carried out by mounting the samples on a 4 K closed-cycle Helium cryostat manufactured by Cryo Industries of America. The samples were excited using a Photon Systems quasi-CW 20 mW 224 nm He-Ag Laser as the excitation source.

2.1. Growth by MBE

Prior to the deposition, c-plane substrates were out-gassed sequentially at 140 °C and 400 °C in the entry chamber and the preparation chamber of the MBE system respectively, till a background pressure of 5×10^{-9} T was reached. The growth was carried out at a substrate temperature of 800 °C, which is higher than that typically employed by other MBE groups [13,14]. The schematic of typical structures investigated in this work is presented in Fig. 1.

Growth was initiated by nitridation of the sapphire at 800 °C, that is exposing the substrate to the active nitrogen for 60 min to convert the

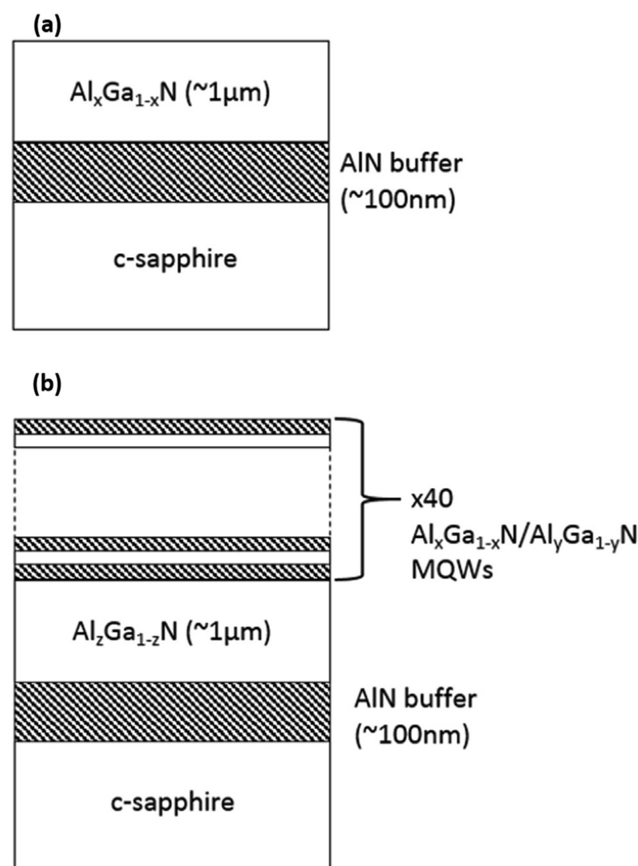

Fig. 1. Schematic of (a) Bulk AlGaN structure (B1) and (b) MQW structures examined in this work (x = z for W1 and W2, x < z for W3, W4 and W5).

topmost layers of the sapphire (Al_2O_3) substrate to AlN, using an RF plasma power of 400 W, and a flow rate of 1.7 sccm, which generated a pressure of 1×10^{-5} T in the growth chamber. An AlN buffer layer was subsequently deposited under the same plasma condition, using a modified migration enhanced epitaxy process as described in a previous work [9]. Choice of the group III–V flux ratio for the buffer layer was driven by several considerations. These include both the crystal quality and smoothness of the surface, as obtained by RHEED, as well as the transparency of the AlN buffer layer, which is quite critical for the development of bottom emitting devices. Typically, streaky RHEED patterns with 2×2 surface reconstructions were observed after the deposition of the AlN buffer layer employing a range of Al fluxes. However, it has been observed that for slightly higher Al fluxes the transparency was dramatically reduced, and there exists a very narrow range of deposition conditions that allow high UV transparencies without significant reduction in crystal quality [15]. In this work, subsequent to the deposition of AlN buffer layer, typically 1 μm thick undoped AlGaN layers were grown, to reduce the dislocation densities and to maintain a stable surface morphology which was then replicated in the subsequent layers. A series of samples were grown where MQWs with AlGaN alloys both in the well and the barrier layers were deposited on to the AlGaN film. Surface and interface morphology were monitored in real-time using the RHEED pattern. Variations were made both in the group III to group V flux ratio, as well as in the annealing schemes, as described in the next section.

2.2. Sample details

Using AlN buffer layers, both bulk AlGaN films and AlGaN MQWs were grown for this work, under a range of group III to group V flux ratios. Sample B1 consists of an AlGaN film with a nominal thickness of

1 µm. This sample was grown under conditions close to stoichiometry. For the sample W1, on top of an AlGaN film a set of 40 wells and barriers were deposited. The nominal thicknesses of the wells and barriers were 7 monolayers (ML) and 11 ML respectively, which corresponds to a periodicity of ~4.75 nm. The deposition conditions for the well layer were exactly the same as those used for the underlying bulk. For the barrier layers, a second Al cell was actuated, such that the total Al flux produced from both the effusion cells was close to that necessary for stoichiometric growth of AlN. A Gallium flux was made incident during the deposition of not only the well but also the barrier layers. For sample W2, all conditions were kept the same as that of W1, but the Gallium flux was increased significantly, as described in a subsequent section. For sample W3, the AlN mole fraction for the underlying AlGaN film was increased, while leaving the wells and barriers identical as in the previous sample. This is necessary for emitters where the light must be extracted through the bottom layer.

One additional step was introduced during the deposition of the quantum well structures in W3. Following the deposition of the barrier layers, the growth was interrupted by closing all metal shutters for a period of time t_{clear} leaving the surface exposed to the active nitrogen while maintaining a temperature of 800 °C. For samples W4 and W5, this process of annealing under active nitrogen was carried out for both the wells and the barriers, other things remaining nearly the same as sample W3. W4 was grown under an excess group III regime, while W5 was grown under a stoichiometric regime.

3. Results and discussion

3.1. Bulk AlGaN (B1)

It has been well recorded in literature that the optical properties of AlGaN alloys depend on complex nanoscale phenomena, which in turn are controlled by the deposition conditions employed [16–18]. This is especially true for high Aluminum content films, such as those studied in this work. Furthermore, while the alloy composition for AlGaN films grown under excess group V conditions is given by the ratio of the arriving Ga and Al fluxes, that is not the case for other growth regimes. For excess group III growth, the active nitrogen is preferably consumed by reaction with Al. Thus, the alloy composition is controlled by the ratio of the Al flux employed to that necessary for stoichiometric growth of AlN. This makes it very difficult to determine the alloy composition from the Ga and Al fluxes used. Therefore, in order to benchmark our studies on MQWs deposited on to the AlGaN thin film, a standalone AlGaN film deposited under similar growth temperatures and plasma conditions was initially investigated. The schematic of this structure is given in Fig. 1(a).

Optical transmission measurements were carried out on this sample and the result is shown in Fig. 2(a). A sharp absorption edge was found at 5.3 eV (~234 nm), which corresponds to an AlGaN composition of about ~76% assuming a bowing parameter of 1.3 [19]. PL measurements were carried out on this sample at room temperature, and a single sharp peak was obtained at 261 nm, as shown in Fig. 2(b). The strong red-shift of the luminescence peak is a phenomenon that has been previously recorded in MBE grown samples [20]. The origin of this red-shift has been linked to the presence of compositional inhomogeneities [6,9,21]. The strong red-shift of the PL peak gives rise to an additional technological challenge. The emission peak position is dependent not only on the AlGaN alloy content, that is the AlN mole fraction, but also on the growth conditions that may lead to a variation of the magnitude of the compositional inhomogeneity. Therefore, a simple direct relation between the alloy content as measured by the optical transmission or XRD, and the peak position as measured by the PL is absent. However, for deep UV emission below 225 nm, the red-shift reduces very quickly as the alloy approaches AlN [22].

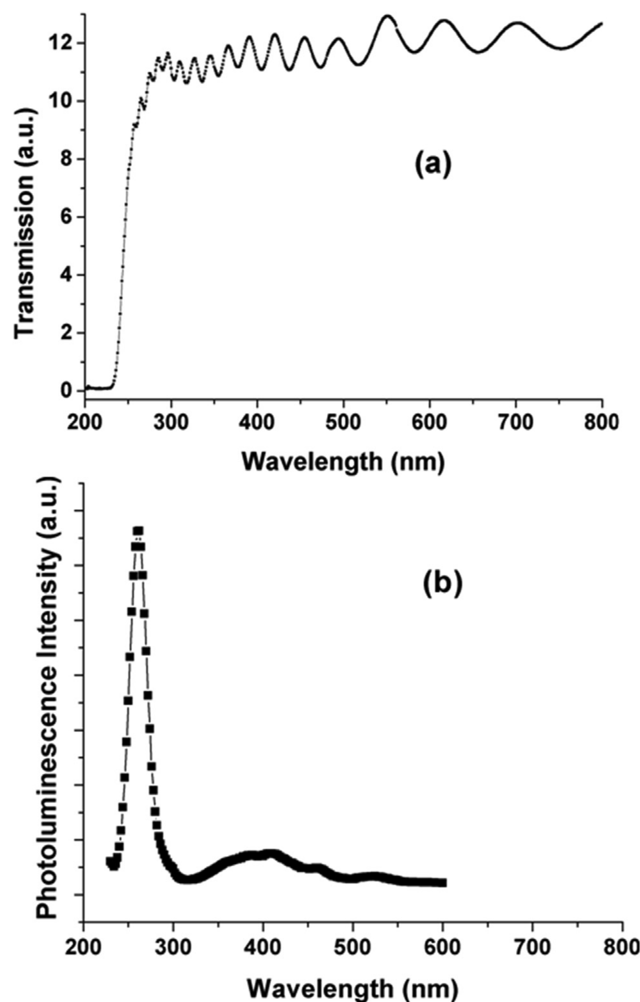

Fig. 2. (a) Optical transmission, and (b) PL spectrum of bulk AlGaN film B1.

3.2. AlGaN MQWs

The optical properties of AlGaN MQWs have been studied extensively as a function of their material properties, especially the alloy composition of the well and the barrier layer. However, the alloy composition is difficult to accurately determine from XRD studies due to strain considerations. Therefore, structures were grown where the initial AlGaN layer was deposited using the same conditions as that employed for the well layers. The number of quantum wells employed in these structures was 40.

Sample W1 has a structure similar to that described in Fig. 1(b). The Ga beam equivalent pressure (BEP) used for the growth of the bulk and MQW layers was 4.5×10^{-7} T. From the in-situ RHEED observations, it was determined that the growth was carried out under an excess group III regime. Fig. 3(a) shows the triple axis 2theta-omega X-ray scans obtained from sample W1. Assuming Vegard's law and the value of AlN and GaN lattice constants obtained from literature [23,24], we determine that the main peak corresponds to (0002) of AlGaN with an AlN mole faction of ~76%. In addition to the peak from sapphire, AlN and AlGaN, two peaks are observed at lower angles, corresponding to the superlattice peaks arising from the MQW structures. Kinematic modelling [25,26] of the structure has been carried out using well and barrier thicknesses of 8 ML and 11 ML respectively. The equation only considers the quantum well and barrier layers and not the bulk AlGaN, buffer AlN and sapphire layers underneath. The main peak observed in the simulated data is the superlattice peak SL0 which is the weighted average of the barrier and wells, assuming no strain, and is located

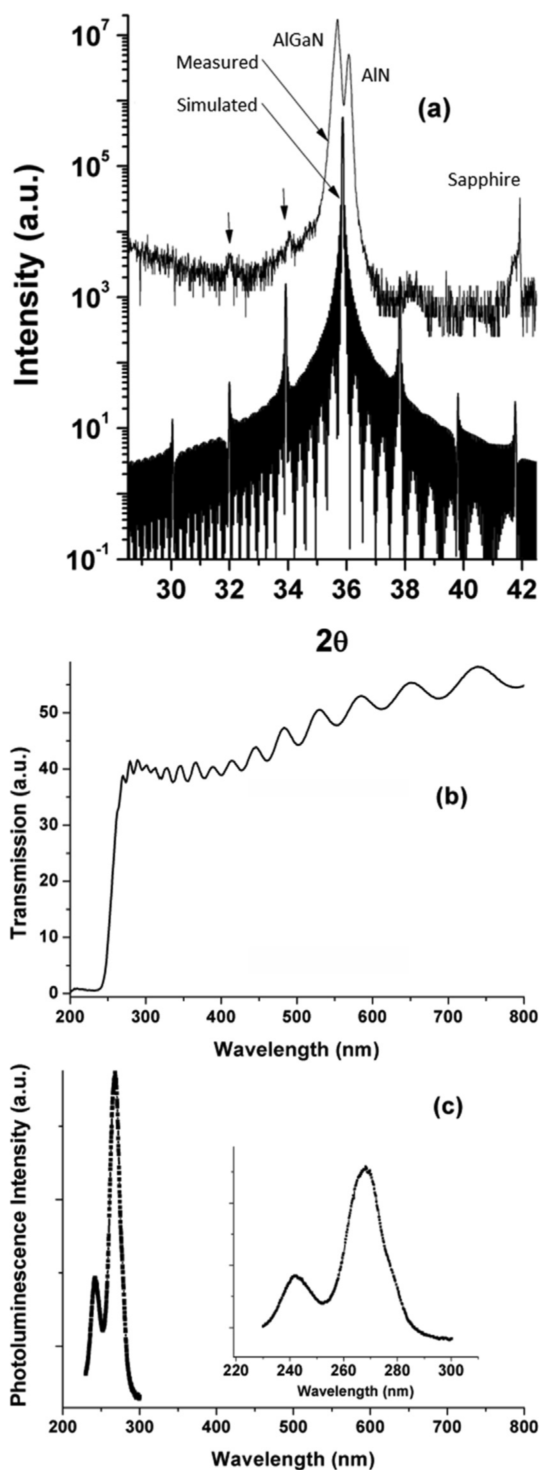

Fig. 3. (a) XRD, (b) Optical Transmission, and (c) Room temperature PL spectrum (inset is in narrower wavelength range) of MQW sample W1.

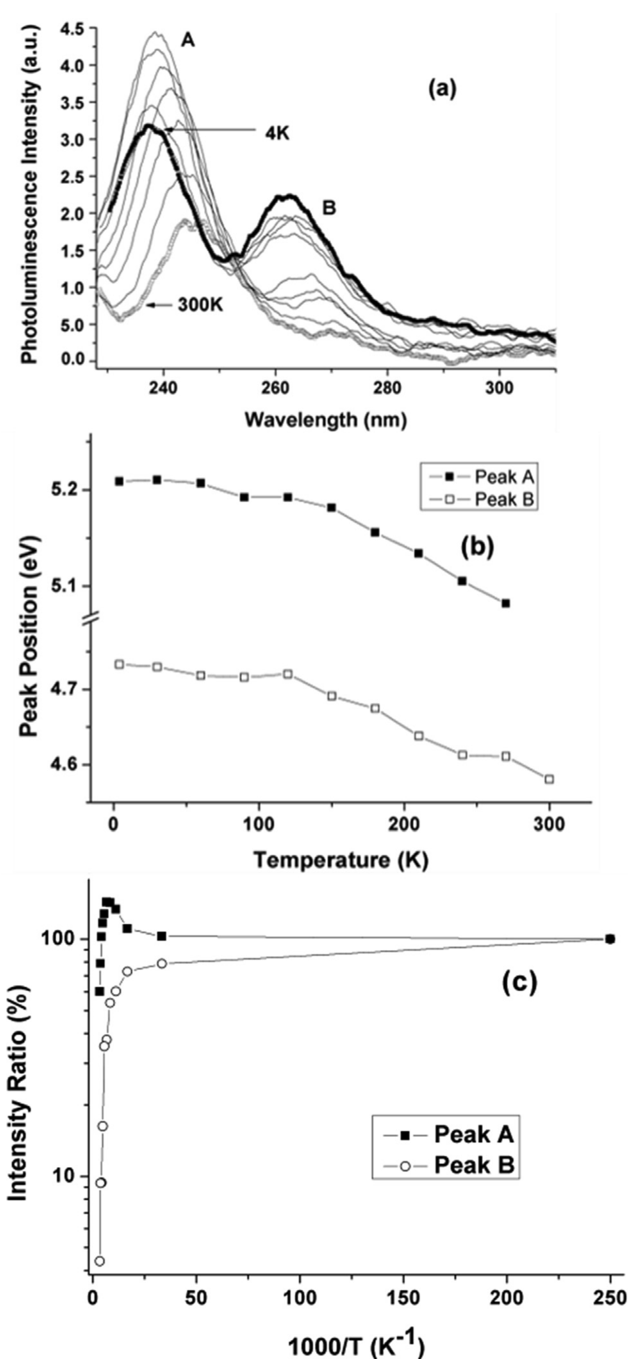

Fig. 4. Temperature dependent PL spectra of MQW sample W2 (a), Temperature dependence of the peak positions (b) and ratio of PL intensity at room temperature to that at 4 K (c) of the two PL peaks.

between the AlN and AlGaN peak. In the experimental data, this peak is overwhelmed by the much stronger and broad peaks from the bulk layers. The other superlattice peaks observed in the experimental data shows a very close match between the experimental and modelled peak positions and we obtain an overall periodicity of 4.75 nm.

Fig. 3(b) shows the transmission spectrum obtained from this sample, which we believe to be dominated by absorption in the bulk AlGaN layer. The absorption edge at 5.06 eV (245 nm), using the values of bowing parameter from Brunner et al. [19], corresponds to ~70% AlN mole fraction. From this result, we are able to estimate the Al BEP required for the stoichiometric growth of AlN. From this value and the BEP employed during growth of barrier layers, we have estimated their alloy composition. This was found to be close to AlN.

Fig. 3(c) shows the room temperature PL data for sample W1. Two distinct peaks can be observed, one around ~236 nm and the other ~268 nm. Comparing this result with Fig. 2(b) the longer wavelength peak can be directly attributed to the bulk film underneath the MQW structures. Thus, the peak at ~236 nm is generated by the overall quantum well structures.

Sample W2 was identical to sample W1 except for the Ga BEP used during the growth of the AlGaN layers, which was significantly larger at 9×10^{-7}T. The PL spectra obtained at room temperature was similar to that from sample W1, except for the intensity of the peak attributed to

the AlGaN MQW region occurring at ~240 nm, which is larger by a factor of 2.4. In order to estimate the IQE for the MQW structures, temperature dependent PL studies were carried out on sample W2, and the results are shown in Fig. 4.

On cooling down from room temperature (300 K) to 4 K the peaks attributed to the quantum wells and the bulk AlGaN show a similar nature in the variation of their peak position. Both the peaks shift to shorter wavelengths, by 6 nm and 8 nm respectively (Fig. 4(b)). However, their variation of intensity with temperature differs significantly. While the luminescence from the bulk AlGaN layer shows a monotonic increase in intensity on cool-down, that from the MQWs increases till the sample reaches a temperature of 150 K, and reduces on further lowering of temperature. The commonly used technique for determination of the IQE is based on temperature dependent luminescence measurement [6,27]. Assuming a 100% radiative recombination at low temperatures, the IQE of the material can be estimated from the ratio of the peak area at room temperature to that at low temperatures. Using this technique for the bulk AlGaN, an IQE of ~4% is obtained.

The temperature dependence of the intensity of the MQW related peak shown in Fig. 4(c) however shows an anomalous behaviour. Instead of a progressive decrease in the intensity with increasing temperature as the carriers get delocalized, thereby increasing the probability of non-radiative recombination through defect states, we observe an increase in intensity till a temperature of ~150 K before the expected reduction. The reduction of PL intensity is observed specifically for quantum well structures and not for bulk films, indicating its link to the presence of potential barriers. Such a temperature dependence has been reported previously [6], and has been attributed to the carriers generated in the region below the MQW layers. Even though a portion of the laser light is absorbed in the quantum wells, significant absorption takes place in the bulk AlGaN films generating electron-hole pairs there. These recombine to form the peak at longer wavelength that is observed in Fig. 4(a). At higher temperatures, part of these carriers diffuses back into the well region and recombine there, thus contributing to the peak at ~240 nm. As the sample is cooled down, these carriers are localized in the AlGaN layer, and recombine from there, increasing the longer wavelength peak, and reducing the peak attributed to the MQWs. Therefore, the IQE cannot be measured directly from this ratio as there is a systematic enhancement of the luminescence at higher temperatures-where the carriers can diffuse back-and undercounting at low temperatures where they cannot. The overall IQE would show an artificial inflation.

This redistribution of carriers indicates that the AlGaN barriers grown under an excess group III regime may allow the percolation of carriers in vertical devices. This has been both theoretically predicted [28] and experimentally shown [29]. While IQE is a prime consideration for the development of UV LEDs, the presence of percolation paths is highly detrimental to the current injection efficiency. Thus, it is critical for all optoelectronic applications that the barriers are efficient in preventing carrier diffusion. This can be increased by (a) increasing the thickness of the barrier, or (b) by reducing the compositional inhomogeneities of the barrier material, or (c) by increasing the abruptness of the interface between the well and barrier layers. For various electronic devices, the thickness of the barriers is determined by the considerations of carrier transport and polarization induced charge generation, and cannot be increased arbitrarily. Fluctuation of the alloy composition of the barrier material, if reduced, can lead to a reduction of in-plane carrier localization and hence radiative recombination. However, the abruptness of the interfaces between the wells and the barriers is also expected to play a very important role in carrier confinement, and in this paper, we address the growth conditions that determine this property.

Growth under an excess group III regime leaves a metallic layer on the growth surface at all times. During the growth of the quantum wells and barriers, this excess metallic layer is left over from the deposition of the previous layer even when the subsequent layer is being grown. The effect is different for the well-barrier and the barrier-well interfaces. In our samples, the barrier layers are very close to AlN. If, due to the drift of the flux during the growth of the barrier layer, the Al layer present on the surface is higher than that can be consumed by the active nitrogen, the excess Al stays on the growth surface and is carried forward to the well growth. The desorption rate of Al being very low and the Al-N bond being significantly stronger than the Ga-N bond, the excess Al necessarily incorporates into the well layer, thereby increasing the AlN mole fraction in initial stages of this layer. If, however the Al content is completely consumed by the active nitrogen in the barrier layer, we expect the barrier-well interface to be abrupt.

However, for the well layer, if the group III–in this case Gallium – is excess, then the metallic layer carries over to the next barrier layer, but is not incorporated in the alloy due to its higher volatility. However, the alloy composition of the layer being deposited at any instant is dependent in a complex fashion on the alloy composition of the metallic layer on the surface, which may not be homogenous. Thus, the well-barrier layer is more difficult to predict but still is probably gradual. In order to improve the interface abruptness, it is thus necessary to ensure that the excess metal on the growth surface from the previous layer is consumed before the deposition of the next layer ensues. In sample W3, after the deposition of each barrier, the growth surface was exposed to the active Nitrogen for a length of time, till a clear RHEED pattern was observed. In samples W4 and W5, similar exposure was carried out after the deposition of both well and barrier layers. In addition, for these three samples, while the quantum well alloy composition was maintained similar to W2, the bulk AlGaN film underneath was grown with significantly more Al content. This was chosen so that the absorption edge of the bulk AlGaN film would be beyond the excitation range of the laser, and thus the PL emission would be generated only from the quantum well layers. However, our optical transmission data indicates that for these high AlN content films, there is considerable band-tailing.

Fig. 5(a) shows the XRD studies carried out on sample W3. In addition to the peak for sapphire, clear superlattice peaks are also observed, which are much stronger than those obtained from W1. These arise from the quantum well structure, and a quantitative analysis by employing the kinematic model shows that the well-barrier periodicity was ~5.5 nm. This is considerably larger than the thickness estimated from growth rates or from sample W1. This can be linked to the active Nitrogen exposure step following the deposition of each barrier layer.

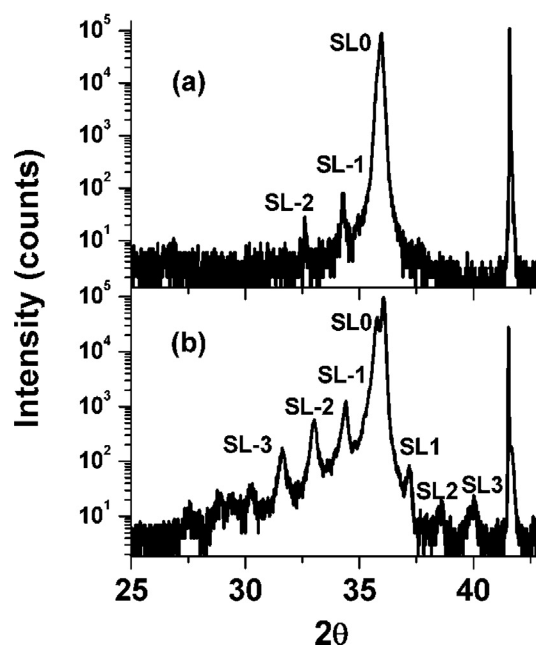

Fig. 5. XRD of MQW samples: (a) W3, and (b) W4.

The barriers were grown under conditions where the Al and Ga fluxes were significantly larger than that required for stoichiometry. Therefore, at the point when the metal shutters were closed, there was a layer of metal on the growth surface, consisting of both Ga and Al. The former easily evaporates at the growth temperature of 800 °C, while the latter does not and is converted into AlN by the active nitrogen, making the barrier width significantly larger than estimated. This does not significantly affect the emission wavelength, but the resulting abruptness of the interface plays a very important role in stopping carrier percolation.

The XRD data presented in Fig. 5(b) shows the superlattice peaks in sample W4, where after growing both the wells and the barrier layers under excess group III conditions, an active nitrogen exposure step was introduced. The results clearly indicate features distinct from that of sample W3. The superlattice peaks are much stronger in this case, and a larger number is clearly observable. Thirdly, from the interval of the superlattice peak, the periodicity was found to be ~6.5 nm, which corresponds to a small increase from W3. This can be linked to the same mechanism as described previously. The sharper superlattice peaks indicate that the interface quality has significantly improved after exposing the well layer as well to the active plasma. Previous reports have indicated that such a step, especially carried out at 800 °C may roughen the surface [30]. This was not the case here as such roughening would reduce and not increase the quality of the interface.

The room temperature PL data from samples W3 and W4 are presented in Fig. 6(a). As explained previously, the peak due to the bulk AlGaN layer is absent from this spectrum, and only the luminescence from the quantum wells can be observed. A single peak is observed for both the samples, with no prominent sub-bandgap luminescence. The PL peaks for both samples show Fabry-Perot fringes that originate from the reflection at the top surface and the sapphire-AlN boundary. This has been substantiated by comparing the PL spectra with the optical transmission data, which show the same fringing. The center of the PL peak for sample W3 is at 241 nm, while the peak from sample W4 is at 248 nm. This variation can be partly explained by the increased thickness of the well and barrier layers as indicated by the XRD data. A more important parameter is the well barrier interface, which is sharp for W4 but diffused for W3. A theoretical model linking the peak position with sharpness of the interface is being developed and will be published elsewhere.

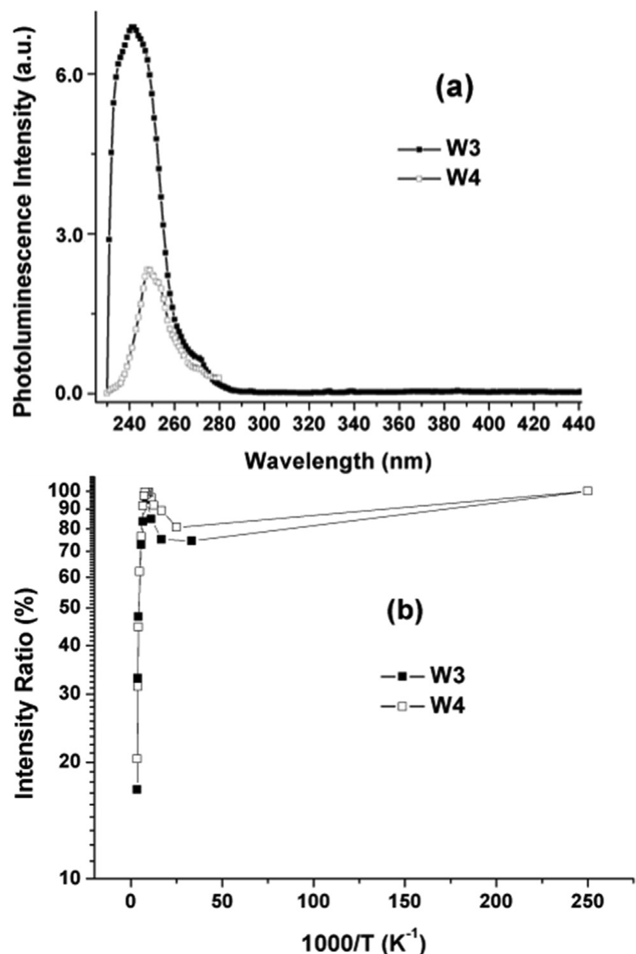

Fig. 6. (a) Room temperature PL spectra of MQW samples W3 (grown with interruption after each barrier) and W4 (grown with interruption after each well and barrier); (b) Comparison of intensity ratios of MQW samples W3 and W4.

A major observation from the room temperature PL measurements is that, contrary to expectations, an increase of interface quality does not translate into a significant increase in brightness. In fact, there is a significant reduction in the PL intensity for sample W4, even though the superlattice peaks in the XRD are stronger and are greater in number. We therefore conclude that the carrier localization, and subsequent radiative recombination in AlGaN quantum wells occurs mostly in the in-plane alloy fluctuations, and the barrier themselves play little role. The improved interface quality however can lead to higher strain and quantum confined Stark effect, which separates the carriers and reduces the probability of radiative recombination.

The temperature dependent PL for these samples are presented in Fig. 6(b) and show similar anomalous behaviour as observed for the MQWs in sample W2. We again attribute these results to the diffusion of carriers as explained previously, and a quantitative measurement of IQE is not possible through the ratio of the PL intensity measured at RT to that measured at 4 K. If we compare the results qualitatively, we find that the intensity ratio $I_{(300K)}/I_{(4K)}$ measured for sample W2 is three times the ratios measured for samples W3 and W4. It appears from these results that the radiative recombination rate is significantly higher for sample W2 than the samples W3 and W4. One possible reason is that for sample W2, the underlying AlGaN being at nearly the same composition as the well layer caused the wells to be completely relaxed, which is not the case for samples W3 and W4.

Sample W5 was grown using a similar structure as employed for W3 and W4, but with a group III to group V flux ratio that is close to stoichiometry. For this sample we have also introduced the exposure step after both the well and the barrier layers. Under these conditions, the surface morphology is rough and faceted as indicated by a representative RHEED pattern shown in Fig. 7(a). Comparison of the XRD pattern for samples W4 and W5 indicates similar periodicity for the two samples. However, the superlattice peaks for sample W5 are relatively less distinct (inset of Fig. 7(b)).

Temperature dependent PL measurements indicate however that the intensity ratio for the sample W5 (Fig. 7(b)) is a significant improvement over that of W4 or W3. The room temperature PL intensity for this sample, as shown in Fig. 8(a), also shows a significant improvement. Therefore, for this sample, a deposition condition has been identified that simultaneously improves the interface quality, as indicated by the XRD, the room temperature PL intensity, as well as the radiative recombination probability as roughly estimated from the intensity ratio. We believe this is due to the reduced surface diffusion length of Al under nearly stoichiometric conditions, which also causes a compositional inhomogeneity and therefore carrier localization. Several groups have reported that bombardment of the growth surface of MBE grown GaN to active Nitrogen plasma or growth under an excess Nitrogen regime results in the formation of V-pits and inverted pyramids on the sample surface [30,31]. These stem from point defects and threading dislocations in the crystal structure. It is possible that an exposure of samples grown under a stoichiometric regime to Nitrogen plasma, as is the case in W5, will result in similar defects. It is well known that the presence of V-defects results in an increase in the IQE of the material

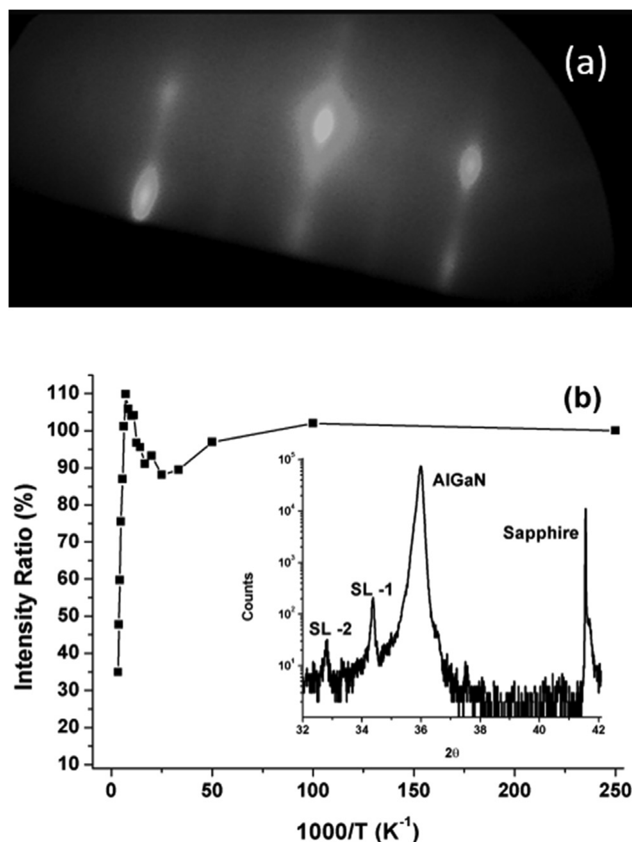

Fig. 7. RHEED pattern indicating rough and faceted surface (a), Ratio of PL intensities at room temperature to that at low temperature of sample W5 (Inset: XRD of W5) (b).

[32,33]. Alternatively, the growth of MQWs on faceted surfaces tilt the interfaces away from the 0001 plane, thereby reducing quantum confined Stark effect. However extensive studies are necessary before we can pinpoint the exact reason for the phenomena.

An interesting observation is made when the PL intensities at room temperature for all the MQW samples are compared. Fig. 8(a) shows a comparative plot of the PL peak height at room temperature for the four samples. Since the intensity ratio can not be directly linked to the numerical value of the IQE, we present the relative measure for the four samples compared to W2, in Fig. 8(b). It is seen that the sample with the highest intensity ratio has the lowest brightness at room temperature. As the emission at room temperature depends both on the IQE as well as the extraction efficiency of the sample, it appears that samples with higher IQE have lower extraction efficiency. While at this point it is difficult to come to any definite conclusion, this may be linked to the fact that a higher group III flux leads to a higher degree of compositional inhomogeneity, and therefore carrier localization away from defect states. However, this also leads to smoother surfaces, which narrows down the emission cone. This is not the case for sample W5 which is rough, and therefore both parameters are increased for this sample.

4. Conclusion

Growth of AlGaN MQWs has been carried out by PA-MBE for use in deep UV emitters. Two different growth regimes have been compared in this work, the near stoichiometric and the excess group III. Our results indicate that growth under excess group III conditions leads to higher radiative recombination rates due to carrier localization in potential fluctuations created by this growth mode. However, the well-barrier interface is quite diffuse and in actual devices there will be substantial inefficiencies arising from percolation of carriers out of the active layers.

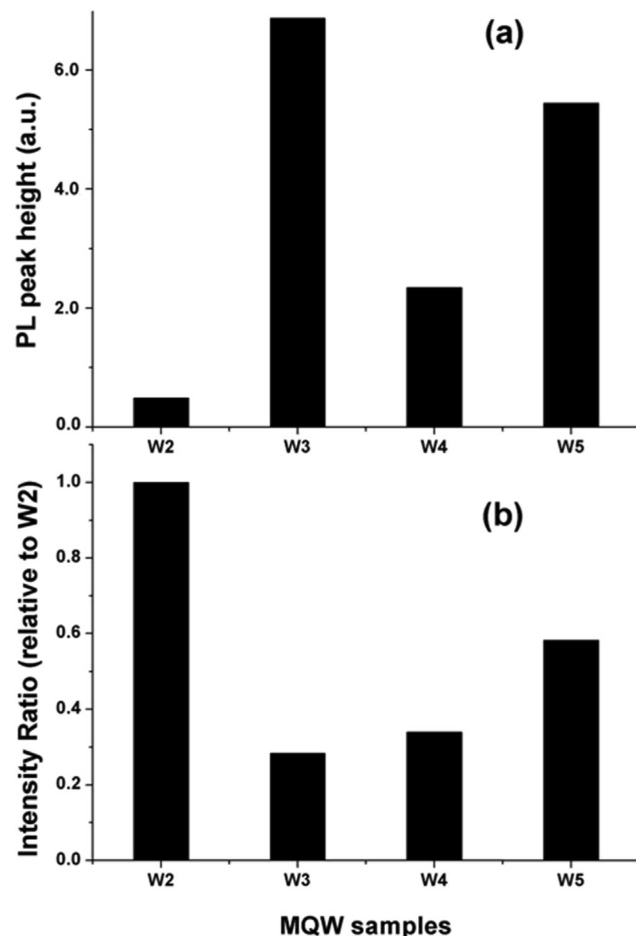

Fig. 8. Comparison of (a) brightness of PL emission at room temperature and (b) intensity ratio of the various MQW samples relative to W2.

A growth technique of incorporating a Nitrogen exposure step has been introduced, after both the well and barrier layer deposition. A significant improvement of well-barrier interface quality has been observed, as indicated by the presence of strong superlattice peaks in the XRD pattern. However, such an improvement does not translate to any improvement of luminescence properties, and the intensity ratio, indicative of the IQE, shows a decrease.

The near-stoichiometric growth conditions - that is typically avoided during PA-MBE growth of MQWs due to increased surface roughness - along with the growth interruption after well and barrier layers, was found to increase the intensity ratio while still maintaining good well-barrier interface quality. These conditions of growth lead to relatively bright quantum well structures, while reducing the carrier leakage. Furthermore, these conditions are better suited for large production systems, where maintenance of a particular group III to group V flux ratio, larger than unity, would be technologically challenging. Our results indicate that the radiative recombination efficiency can be improved by either an introduction of a controlled level of compositional inhomogeneity by use of excess group III conditions during growth, or by use of faceted well-barrier interfaces by using stoichiometric conditions and plasma exposure steps after well and barrier layers.

Declaration of Competing Interest

None declared.

Acknowledgments

This work was partially funded by the Office of the Principal Scientific Advisor, Government of India (Prn SA/W-UV LEDS/2017). SS (09/028 (0921)/2014-EMR-I) and AD (09/028(0946)/2015-EMR-I) would like to acknowledge the Council of Scientific and Industrial Research Senior Research Fellowship (CSIR-SRF) scheme, CS (IF120257) would like to acknowledge the Department of Science and Technology (DST) INSPIRE fellowship, AS would like to acknowledge the UGC Rajiv Gandhi National Fellowship scheme and PP (PDF/2017/001605) would like to thank the Science and Engineering Research Board (SERB) National Post-Doctoral Fellowship (NPDF) scheme for funding their work.

References

[1] Y. Muramoto, M. Kimura, S. Nouda, Semicond. Sci. Technol. 29 (2014) 084004, https://doi.org/10.1088/0268-1242/29/8/084004.
[2] P. Specht, C. Kisielowski, Mater. Sci. Semicond. Process. 65 (2017) 24, https://doi.org/10.1016/j.mssp.2016.07.011.
[3] A.M. Sanchez, M. Gass, A.J. Papworth, P.J. Goodhew, P. Singh, P. Ruterana, H.K. Cho, R.J. Choi, H.J. Lee, Thin Solid Films 479 (2005) 316, https://doi.org/10.1016/j.tsf.2004.11.207.
[4] V.G. Deibuk, A.V. Voznyi, Semiconductors 39 (2005) 623.
[5] J. Mickevicius, G. Tamulaitis, M. Shur, M. Shatalov, J. Yang, R. Gaska, Appl. Phys. Lett. 101 (2012) 211902, https://doi.org/10.1063/1.4767657.
[6] Y. Liao, C. Thomidis, Chen-kai Kao, T.D. Moustakas, Appl. Phys. Lett. 98 (2011) 081110, https://doi.org/10.1063/1.3559842.
[7] J.S. Cabalu, A. Bhattacharyya, C. Thomidis, I. Friel, T.D. Moustakas, C.J. Collins, Ph. Komninou, J. Appl. Phys. 100 (2006) 104506, https://doi.org/10.1063/1.2388127.
[8] D. Korakakis, K.F. Ludwig Jr., T.D. Moustakas, Appl. Phys. Lett. 71 (1997) 72, https://doi.org/10.1063/1.119916.
[9] P. Pramanik, S. Sen, C. Singha, A.S. Roy, A. Das, S. Sen, A. Bhattacharyya, J. Appl. Phys. 120 (2016) 144502, https://doi.org/10.1063/1.4964420.
[10] M.A. Sanchez-Garcia, E. Calleja, E. Monroy, F.J. Sanchez, F. Calle, E. Munoz, R. Beresford, J. Cryst. Growth 183 (1998) 23.
[11] A.V. Sampath, G.A. Garrett, C.J. Collins, W.L. Sarney, E.D. Readinger, P.G. Newman, H. Shen, M. Wraback, J. Electron. Mater. 35 (2006) 641.
[12] E.J. Tarsa, B. Heying, X.H. Wu, P. Fini, S.P. DenBaars, J.S. Speck, J. Appl. Phys. 82 (1997) 5472, https://doi.org/10.1063/1.365575.
[13] S. Matta, J. Brault, M. Korytov, T.Q.P. Vuong, C. Chaix, M.A. Khalfioui, P. Vennéguès, J. Massies, B. Gil, J. Cryst. Growth 499 (2018) 40, https://doi.org/10.1016/j.jcrysgro.2018.07.023.
[14] S.W. Kaun, B. Mazumder, M.N. Fireman, E.C.H. Kyle, U.K. Mishra, J.S. Speck, Semicond. Sci. Technol. 30 (2015) 055010, https://doi.org/10.1088/0268-1242/30/5/055010.
[15] T. Suzuki, H. Yaguchi, H. Okumura, Y. Ishida, S. Yoshida, Jpn. J. Appl. Phys. 39 (2000) L497.
[16] A.V. Sampath, G.A. Garrett, R.W. Enck, P. Rotella Jr., H. Shen, M. Wraback, Phys. Status Solidi C 8 (2011) 1534, https://doi.org/10.1002/pssc.201001167.
[17] P. Pramanik, S. Sen, C. Singha, A.S. Roy, A. Das, S. Sen, A. Bhattacharyya, D. Kumar, D.V.S. Rao, J. Cryst. Growth 439 (2016) 60, https://doi.org/10.1016/j.jcrysgro.2016.01.004.
[18] C. Singha, S. Sen, P. Pramanik, M. Palit, A. Das, A.S. Roy, S. Sen, A. Bhattacharyya, J. Cryst. Growth 481 (2018) 40, https://doi.org/10.1016/j.jcrysgro.2017.10.027.
[19] D. Brunner, H. Angerer, E. Bustarret, F. Freudenberg, R. Hopler, R. Dimitrov, O. Ambacher, M. Stutzmann, J. Appl. Phys. 82 (1997) 5090, https://doi.org/10.1063/1.366309.
[20] C.J. Collins, A.V. Sampath, G.A. Garrett, W.L. Sarney, H. Shen, M. Wraback, A.Yu. Nikiforov, G.S. Cargill III, V. Dierolf, Appl. Phys. Lett. 86 (2005) 031916, https://doi.org/10.1063/1.1856702.
[21] E. Monroy, N. Gogneau, F. Enjalbert, F. Fossard, D. Jalabert, E. Bellet-Amalric, Le Si Dang, B. Daudin, J. Appl. Phys. 94 (2003) 3121, https://doi.org/10.1063/1.1598633.
[22] G. Coli, K.K. Bajaj, J. Li, J.Y. Lin, H.X. Jiang, Appl. Phys. Lett. 80 (2002) 2907, https://doi.org/10.1063/1.1471932.
[23] S. Iwama, K. Hayakawa, T. Arizumi, J. Cryst. Growth 56 (1982) 265, https://doi.org/10.1016/0022-0248(82)90443-2.
[24] V. Bougrov, M. Levinshtein, S. Rumyantsev, A. Zubrilov, Gallium Nitride (GaN), in: M.E. Levinshtein, S.L. Rumyantsev, M.S. Shur (Eds.), Properties of Advanced Semiconductor Materials, John Wiley and Sons, New York, 2001, p. 2.
[25] D. Korakakis, K.F. Ludwig Jr., T.D. Moustakas, Appl. Phys. Lett. 72 (1998) 1004, https://doi.org/10.1063/1.120976.
[26] D.B. McWhan, Synthetic Modulated Structures, Academic, Orlando, 1985 Chap. 2.
[27] Y. Xing, L. Wang, Z. Wang, Z. Hao, Y. Luo, C. Sun, Y. Han, B. Xiong, J. Wang, H. Li, J. Appl. Phys. 122 (2017) 135701, https://doi.org/10.1063/1.5005619.
[28] Hung-Hsiang Chen, J.S. Speck, C. Weisbuch, Yuh-Renn Wu, Appl. Phys. Lett. 113 (2018) 153504, https://doi.org/10.1063/1.5051081.
[29] P. Pramanik, S. Sen, C. Singha, A.S. Roy, A. Das, S. Sen, D.V.S. Rao, A. Bhattacharyya, IEEE J. Quant. Electron. 52 (2016) 4300206, https://doi.org/10.1109/JQE.2016.2516445.
[30] B. Heying, R. Averbeck, L.F. Chen, E. Haus, H. Riechert, J.S. Speck, J. Appl. Phys. 88 (2000) 1855, https://doi.org/10.1063/1.1305830.
[31] R.J. Molnar, T.D. Moustakas, J. Appl. Phys. 76 (1994) 4587.
[32] A. Hangleiter, F. Hitzel, C. Netzel, D. Fuhrmann, U. Rossow, G. Ade, P. Hinze, PRL 95 (2005) 127402, https://doi.org/10.1103/PhysRevLett.95.127402.
[33] Shuo-Wei Chen, Heng Li, Chia-Jui Chang, Lu. Tien-Chang, Materials 10 (2017) 113, https://doi.org/10.3390/ma10020113.